Free-Standing Faradaic Motors Based on Biocompatible Nanoperforated Polylactic Acid Layers and Electropolymerized Poly(3,4-ethylenedioxythiophene)

Brenda G. Molina,[1,2] Sergi Cuesta,[1,2] Hossein Besharatloo,[2,3] Joan Josep Roa,[2,3] Elaine Armelin,[1,2] and Carlos Alemán[1,2,4*]

[1] *Departament d'Enginyeria Química, EEBE, Universitat Politècnica de Catalunya, C/ Eduard Maristany 10-14, Ed. I2, 08019 Barcelona, Spain*

[2] *Barcelona Research Center for Multiscale Science and Engineering, Universitat Politècnica de Catalunya, Eduard Maristany 10-14, 08019 Barcelona, Spain*

[3] *CIEFMA-Departament de Ciència dels Materials i Eng. Metal·lúrgica, Universitat Politècnica de Catalunya, Eduard Maristany 10-14, Ed. I, 08019 Barcelona, Spain*

[4] *Institute for Bioengineering of Catalonia (IBEC), The Barcelona Institute of Science and Technology, Baldiri Reixac 10-12, 08028 Barcelona, Spain*

[*] Corresponding author: carlos.aleman@upc.edu

ABSTRACT

The electro-chemo-mechanical response of robust and flexible free-standing films made of three nanoperforated poly(lactic acid) (pPLA) layers separated by two anodically polymerized poly(3,4-ethylenedioxythiophene) (PEDOT) layers, has been demonstrated. The mechanical and electrochemical properties of these films, which are provided by pPLA and PEDOT, respectively, have been studied by nanoindentation, cyclic voltammetry and galvanostatic charge-discharge assays. The unprecedented combination of properties obtained for this system is appropriated for its utilization as a Faradaic motor, also named artificial muscle. Application of square potential waves has shown important bending movements in the films, which can be repeated for more than 500 cycles without damaging its mechanical integrity. Furthermore, the actuator is able to push a huge amount of mass, as it has been proved by increasing the mass of the passive pPLA up to 328% while keeping unaltered the mass of electroactive PEDOT.

Keywords: Actuator; Artificial muscle; Conducting polymer; Nanoindentation

INTRODUCTION

Electro-chemo-mechanical artificial muscles made of electroactive polymeric films are motors driven by reversible electrochemical reactions (Faradaic motors).[1,2] Thus, electrons are extracted from or injected to polymeric chains during the reactions generating positive or negative chains, respectively, while hydrated counterions (*i.e.* anions or cations accompanied with water molecules) are exchanged between the polymeric matrix and the electrolyte to keep the charge balance inside the film (Figure 1a). Such electronic and ionic charge transport processes cause the conformational movements of the polymer chains that, together with the compositional variation inside the polymeric matrix (*i.e.* entrance and scape of hydrated ions), guarantee the film volume variation during reversible oxidation and reduction reactions (swelling and shrinking, respectively). These physical and chemical events (*i.e.* electric pulse, chemical reaction, conformational movements, ions and water exchange, and volume variation) resemble those taking place in natural muscles during the contraction and, therefore, the electrochemically driven reversible variations of the film volume are used to construct Faradaic electrochemical devices.[3-5]

Bending artificial muscles based on electrochemical reactions have been mainly developed for conducting polymers (CPs),[4-6] carbon nanotubes[7,8] and graphenes.[9,10] Among them, the most studied are the bilayers made of CP/tape,[3,4] CP/metal,[11,12] CP/plastic,[13] in which the second layer acts as a passive element transforming the volume variation induced by the electrochemical energy into mechanical energy through a bending movement. Besides, interpenetrated polymer networks,[14-16] with bending movements higher than ±30º, and asymmetric bilayer made of two different conducting polymers[17-19] have been also successfully developed. Other approaches have been used to construct electromechanical actuators for specific applications. For example, in the

field of elastic voltage controlled artificial muscles, CPs have been grafted to soft block copolymers to produce elastomer-like materials capable of more than 150% actuation strain.[20,21] Agrawal *et al.*[22] dispersed carbon black nanoparticles in a liquid crystal elastomer network to produce conductive nanocomposites and promote cell viability by applying electromechanical stimuli. More recently, Lee *et al.*[23] reported on Micro-ElectroMechanical (MEM) 3D-printed switches using conductive poly(lactic acid) with excellent mechanical actuation characteristics. Excellent reviews summarizing all these advances have been recently reported.[1,24-27]

In this work we present a smart approach that synergistically combine the mechanical advantages of free-standing (also named self-supported) poly(lactic acid) (PLA) ultra-thin films and the electrochemical response of anodically polymerized CPs to produce effective multilayered Faradaic motors. More specifically, free-standing 5-layered films consisting of three nanoperforated PLA (pPLA) ultra-thin films separated by two nanolayers of poly(3,4-ethylenedioxythiophene) (PEDOT), hereafter denoted 5-pPLA/PEDOT (Figure 1b), fulfil the mechanical and electrochemical requirements of artificial actuators. Square potential waves have been used to induce bending movements in free-standing 5-pPLA/PEDOT films. Furthermore, the influence of the potential and the mass of electrochemically inert PLA on the cycle stability and amplitude of movement of the films has been analyzed. It is worth noting that both PLA and PEDOT are biocompatible polymers currently used in a huge amount of biomedical applications (*e.g.* in scaffolds, drug delivery and antimicrobial systems, tissue regeneration),[28-36] thus, results derived from this work open new possibilities for engineering multifunctional biomedical devices. For example, devices based on 5-pPLA/PEDOT functionalized at the top layer with porin proteins are expected to to convert the energy associated to the transport of metabolites in a Faradaic motor.

EXPERIMENTAL METHODS

Materials. Poly(3-ethylenedioxythiophene) : polystyrene sulfonate (PEDOT:PSS) 1.3 wt. % dispersion in H_2O, 3,4-ethylenedioxythiophene (EDOT), polyvinyl alcohol (PVA) 87-89% hydrolyzed, and lithium perchlorate ($LiClO_4$) were purchased from Sigma-Aldrich (USA). Polylactic acid (PLA) 2002D, a product of Natureworks, was kindly supplied by Nupik International (Polinyà, Spain). According to the manufacturer, this PLA has a D content of 4.25%, a residual monomer content of 0.3%, density of 1.24 g/cm^3, glass transition temperature (T_g) of 58 $^{\circ}$C, and melting temperature (T_m) of 153 $^{\circ}$C. Acetonitrile and hexafluoroisopropanol (HFIP) were purchased from Panreac Quimica S.A.U. (Spain).

Fabrication of free-standing 5-pPLA/PEDOT membranes. Free-standing 5-layered membranes were prepared adapting an already reported procedure.[37] A PEDOT:PSS layer followed by a nanoperforated PLA (pPLA) layer, both spin-coated onto steel substrate (AISI 304 sheet of 3×3 cm^2), were used as working electrode for the anodic polymerization of PEDOT. pPLA layers were obtained by blending PLA and PVA with a ratio of 90:10 v/v (PLA:PVA), prepared by mixing PLA (10 mg/mL) and PVA (10 mg/mL) HFIP solutions, and removing PVA domains via solvent etching. Spin-coating was performed using the 1200 rpm for 60 s with a spin-Coater (WS-400BZ-6NPP/A1/AR1 Laurell Technologies Corporation).

PEDOT was electropolymerized by chronoamperometry in a tree-electrode cell under a constant potential of +1.40 V and adjusting the polymerization charge to 270 mC. Chronoamperometries were performed using a VersaStat II potenciostat-galvanostat connected to a computer controlled through a Power Suite Princenton Applied Research program. The cell was filled with 40 mL of a 10 mM EDOT solution

in acetonitrile containing 0.1 M $LiClO_4$ as supporting electrolyte. The reference electrode was an Ag|AgCl electrode containing a KCl saturated aqueous solution (E^o = 0.222 V at 25 ºC), while the counter electrode was a bare steel AISI 316L sheet.

The combination of spin-coating and electropolymerization techniques was used to prepare 5-layered films, which alternate pPLA and PEDOT ultra-thin sheets, separated from the steel substrate by PEDOT:PSS sacrificial layer. Thus, the composition of such supported 5-layered films was pPLA/PEDOT/pPLA/PEDOT/pPLA, hereafter abbreviated 5-pPLA/PEDOT. Detachment of the 5-layered films from the steel substrate was achieved by selective elimination of the PEDOT:PSS sacrificial layer. Although PEDOT:PSS is not soluble in water, it forms a colloidal dispersion. After immersion into milli-Q water for 12 h, 5-layered films were detached from the steel substrate with tweezers.

Profilometry. Film thickness measurements were carried out using a Dektak 150 stylus profilometer (Veeco, Plainview, NY). Different scratches were intentionally caused on the films and measured to allow statistical analysis of data. At least eighteen independent measurements were performed for three samples of each examined condition. Imaging of the films was conducted using the following optimized settings: tip radius= 12.5 μm; stylus force= 3.0 mg; scan length= 1 mm; and speed= 100 μm/s.

Scanning electron microscopy (SEM). A Focus Ion Beam Zeiss Neon 40 instrument (Carl Zeiss, Germany) equipped with an energy dispersive X-ray (EDX) spectroscopy system and operating at 5 kV for characterization of the membranes was used. Films supported onto steel sheets were mounted on a double-sided adhesive carbon disc and sputter-coated with an ultra-thin carbon layer (6-10 nm) to prevent sample charging

problems. The diameter of the perforations was measured with the SmartTiff software from Carl Zeiss SMT Ltd.

Nanoindentation. The mechanical response (hardness and elastic modulus) of the coating at the micro- and submicrometric length scale was studied by means of the nanoindentation technique. Nanoindentation tests were performed by using a Nanoindenter XP (MTS) with a Berkovich diamond indenter. This equipment worked with continuous stiffness measurement mode (CSM), allowing a dynamic determination of the mechanical properties during the indentation process. It was used a homogeneous array of sixteen imprints (four by four) working under displacement control mode. The tests were conducted at 100 nm of maximum displacement into surface to determine the coating mechanical properties in terms of hardness and elastic modulus. The distance between imprints was held constant and equal to 5 μm in order to avoid any overlapping effect. Such conditions guarantee that each individual test could be treated as an independent statistical event. The strain rate was held constant at 0.05 s^{-1} and the shape of the indenter tip was carefully calibrated by indenting a fused silica standard of well-known Young's modulus (72 GPa). In order to get the hardness and the elastic modulus, the obtained data were analyzed by using the Oliver and Pharr equations as previously reported.[38,39].

Electrochemical assays. All the electrochemical assays were performed using the Autolab PGSTAT302N and Nova software. Experiments were conducted in $LiClO_4$ 0.1 M aqueous solution at room temperature. A conventional Ag|AgCl 3 M KCl electrode and a platinum wire were used as reference electrode and counter electrode, respectively. Cyclic voltammograms were recorded with an initial and final potential of

−0.20 V and +0.60 V. Galvanostatic charge/discharge (GCD) cycles were applied to evaluate the durability of the membrane when submitted to electrochemical stress. More specifically, 1500 GCD cycles were applied at a current density of 1.05 mA/g with a cell voltage comprised between −0.20 V and +0.6 V.

Electro-mechanical assays. The electro-mechanical response was measured applying a square signal of 0.6, 1, 2, 3 or 4 V for a time comprised between 2 and 10 s. The first half of the time (*e.g.* first 5 s in the case of 10 s) were with a positive voltage to oxidize the sample while the last 5 s were with negative voltage to reduce it (Figure S1). The movement with increasing weights was examined. For this purpose, the weight of the outer pPLA layer was increased by decreasing the spin coating rate to 900, 600, 300 and 100 rpm during 60 s.

Images were captured with the digital microscope Dino-Lite AM7013MZT previously calibrated. The area of each sample before and after stimulus was measured by the software Image J. All the experiments were repeated three times.

RESULTS AND DISCUSSION

Self-standing 5-pPLA/PEDOT membranes were prepared adapting an already reported procedure,[37] which is sketched in Figure 2. In brief, a sacrificial layer of 302±3 nm thickness was obtained onto a steel AISI 304 sheet of 3×3 cm^2 by spin-coating using a commercial aqueous solution of PEDOT doped with polystyrene sulfonate (PEDOT:PSS). Then, a pPLA layer was spin-coated onto the sacrificial layer. This was achieved by spin-coating a mixture of PLA and PVA. As these are immiscible polymers, the formation of spherical nanofeatures was induced by phase segregation (*i.e.* segregated nanodomains). The diameter of such nanofeatures was adjusted to the entire film

thickness by regulating the operational conditions of the spin-coating process (*i.e.* time and angular speed) and the concentration of the less abundant polymer (PVA) in the feeding mixture (see Methods section in the ESI). After this, selective water etching was applied to dissolve the less abundant PVA, transforming the formed nanofeatures into nanoperforations while PLA remained unaltered.

The resulting PEDOT:PSS/pPLA bilayer was used as working electrode for the anodic polymerization of PEDOT doped with ClO_4^-. In all cases, pPLA layers were obtained by blending PLA and polyvinyl alcohol (PVA) with a ratio of 90:10 v/v, and removing PVA domains via water etching. PEDOT was anodically polymerized using a constant potential of +1.40 V and adjusting the polymerization charge to 270 mC. As it was proved in previous work,[37] the anodic polymerization is successful due to the nanoperforations of the PLA layer, which allow the 3,4-ethylenedioxythiophene (EDOT) monomer to reach the internal semiconducting layer (*i.e.* PEDOT:PSS sacrificial layer or the previously electropolymerized PEDOT layer). This process was repeated until the 5-layered film made of three pPLA layers separated by two anodically polymerized PEDOT layers was obtained (Figure 2).

As determined by contact profilometry, the thickness of pPLA layers was approximately half of the thickness of PEDOT layers. More specifically, the thickness of the 1st (adhered to the sacrificial layer), 3rd (intermediate) and 5th (external) pPLA layer was 95±4, 94±7 and 114±9 nm, respectively, while the 2th an 4th PEDOT layer exhibited a thickness of 210±19 and 199±18 nm, respectively. Accordingly, the thickness of the whole 5-layered film is around 0.7 μm, which is distributed in ~0.3 μm and ~0.4 μm for the nPLA and PEDOT layers, respectively. Finally, the 5-pPLA/PEDOT film was detached from the steel substrate by immersion into milli-Q water for 12 h. More details

about the procedure are provided in the Electronic Supporting Information, while the success of each step was proved in previous work.[37]

Figure 3a shows a representative supported 5-pPLA/PEDOT membrane with area of 3×2 cm^2 prepared for this work. This membrane is cut and converted into six self-standing membranes with area of 2×0.5 by elimination of the sacrificial layer. Figure 3a also displays three of the resulting self-standing membranes floating in water. An average film thickness of 725±60 nm was obtained by profilometry scratching. Membranes were stable on air and in water solution for their manipulation, stability that remained after months from their preparation. Rounded-shape nanoperforations at the surface of the supported 5-pPLA/PEDOT membrane are shown in the Figure 3b, which exhibits a representative SEM micrograph. The diameter of the nanoperforations, which allow to intuit the globular aspect of the internal PEDOT layer appearing inside them, is 109±34 nm. The internal PEDOT layers are more clearly identified in Figure 3c, which displays the transversal view of a self-standing membrane as well as representative energy dispersive X-ray (EDX) spectra from both surface and the internal regions. As it can be seen, the only elements detected at the surface were carbon and oxygen, which is consistent with the PLA composition, while the peak of sulfur corresponding to PEDOT is clearly identified at the spectrum of the internal region. Detailed structural (*i.e.* layer-by-layer SEM and AFM studies) and spectroscopic (*i.e.* layer-by-layer FTIR and Raman studies) characterization of 5-pPLA/PEDOT membranes was provided in our previous manuscript[37] and, therefore, in the rest of this study we have focused on the mechanical, eletrochemical and chemo-electro-mechanical response of the self-standing membrane.

The variation of the micromechanical properties, hardness and elastic modulus, as a function of the indentation depth for the 5-pPLA/PEDOT membrane deposited over commercial steel is presented in Figure 4. In order to evaluate the effect of the substrate,

the micromechanical properties for the substrate steel were determined at the same conditions. Hardness and elastic modulus for the substrate steel employed were found to be 7.05 ± .74 GPa and 216 ± 13 GPa, respectively, at the sub-micrometric length scale. Hardness values are higher than those expected for TRIP steels as reported by Roa *et al.*,[38] whereas elastic modulus values are in satisfactory agreement with those determined by other authors in steels.[40,41]

A clear influence of the substrate for displacement into surface of around 80 and 50 nm for the hardness and elastic modulus, respectively, was found. Furthermore, the hardness and the elastic modulus data present a relatively large scatter due to the heterogeneity of the membrane in terms of local variations and porosity. Three different regions can be clearly observed in Figure 4a: (1) for indents shallower than 30 nm the values are strongly affected by length scale or indentation size effect; (2) penetration depth ranged between 30 to 80 nm, the hardness remains stable and equals to 0.18 ± 0.08 GPa, which may be related with the coating hardness; and (3) for penetration depths higher than 80 nm, the plastic field slightly interacts with the metallic substrate and starts to increase.

As it is shown in Figure 4b, the elastic modulus for the 5-pPLA/PEDOT membrane linearly increases for penetration depths higher than 15 nm due to the elastic field directly interacts with the employed substrate. Within this context, an appropriate model was required in order to deconvolute the substrate effect and be able to determine the elastic modulus for the membrane alone. The Bec *et al.*[42] equation was employed to determine the intrinsic elastic modulus for the membrane:

$$\frac{1}{E_{eff}} = \frac{2 \cdot a}{1 + \frac{2 \cdot t}{\pi \cdot a}} \cdot \left(\frac{t}{\pi \cdot a^2 \cdot E_m} + \frac{1}{2 \cdot a \cdot E_s} \right)$$

where E_{eff} is the effective elastic modulus determined through the equation proposed by Oliver and Pharr,[38] the subindex *m* and *s* refer to membrane and substrate, respectively, *a* is the contact radius, and *t* is the coating thickness. As a result, the membrane elastic modulus was calculated to be 3.4 GPa. This value is about 30 % lower than those presented in the plateau labelled as * in Figure 4b, sustaining then the strong interaction of the elastic field with the substrate.

Figure 5a displays the cyclic voltammograms recorded in 0.1 M $LiClO_4$ aqueous solution for 5-pPLA/PEDOT films supported onto steel as they grow layer-by-layer. As it can be seen, the electroactivity, which is estimated from the cathodic and anodic areas of the voltammograms, is significantly higher for PEDOT layers than for pPLA layers. Obviously, this difference is more pronounced when the 1st pPLA and the 2nd PEDOT layers are compared. Besides, the 3rd pPLA layer exhibits a high electroactivity in comparison with the 1st one since the nanoperforations of the former allow the mobility of dopant ions from the 2nd PEDOT layer. In addition, the electroactivity is higher for the 4th PEDOT layer than for the 2nd one due to nanoperforations in the 3rd pPLA layer.

Figure 5b displays the cyclic voltammogram recorded for a free-standing 5-pPLA/PEDOT film in 0.1 M $LiClO_4$ aqueous solution. The electroactivity is smaller for the free-standing film than for the one supported onto steel. This expected result has been attributed to the difficulties associated with the immobilization of the free-standing membrane onto the electrode, making very difficult the contact between them to be complete once the sacrificial layer has been removed. In spite of this limitation, the electrochemical activity of free-standing 5-pPLA/PEDOT is noticeably high, especially when compared with that of a supported pPLA film (Figure 5b). This electroactivity remains practically unaltered after 25 consecutive oxidation-reduction cycles (*i.e.* reduction of only 4.8%), as is evidenced by the similarity between the two voltammograms (Figure

5b). These results have been attributed to the conducting channels created by PEDOT layers, which can be appreciated in pPLA outer layer (Figures 3b). Although the electroactivity of free-standing 5-pPLA/PEDOT films remains practically intact and the mechanical integrity is apparently preserved after 25 consecutive redox cycles, morphological inspection reveals significant changes in the nanoperforations of the external pPLA layer (Figure 5c). The spherical shape of the nanoperforations is preserved while their average diameter (237±77 nm) increases more than twice with respect to that of as prepared membranes (109±34 nm). This has been attributed to electro-chemo-mechanical effects underwent by the internal PEDOT layers when they are submitted to oxidation and reduction processes. PEDOT layers swells during oxidation by the entrance of hydrated perchlorate anions and shrink during reduction by the expulsion of the same hydrated counter-anions. The continued swelling-shrinking processes experienced by PEDOT layers during the potential scan affect the structure of the flexible upper pPLA layer, increasing the area of pores.

In order to ascertain if the studied free-standing films retain the structure when they are submitted to prolonged electrochemical stress, 1500 galvanostatic charge-discharge (GCD) cycles were run at a current density of 1.05 mA/g in the two-electrode configuration. The cell voltage varied approximately from –0.25 to 0.65 V through each cycle, which corresponds to charge-discharge time of 7.7 seconds. Figure 5d shows the first GDC curves, which apparently present a pseudo-triangular shape with a voltage drop (V_{drop}) of ~0.25 V at the beginning of the discharging step, which is due to internal resistance of the electrode. Detailed inspection of the second GCD cycle in Figure 5e allows appreciating the deviation from the ideal triangle with a voltage drop at a time close 5 s. However, such shape clearly corresponds to that expected for a real electrochemically active conducting polymer, as it is PEDOT.[43,44] After 1500 GCD

cycles both the value of V_{drop} and the shape of the curve remained practically unaltered (Figure 5e), evidencing the lifetime stability 5-pPLA/PEDOT.

As observed above for cyclic voltammetry, consecutive charge-discharge cycles induce structural changes in PEDOT electrodes, which evolve from a compact morphology to a more porous one and vice-versa. This affects the shape and size of the nanoperforations of the external pPLA layer, which become less rounded and much bigger after 1500 GCD cycles (Figure 5f). More specifically, the average diameter increases to 491±215 nm, which represents an increment of around four times with respect to those of as prepared films, and become very heterogeneous, as is proved by the large standard deviation. In spite of this, it is worth noting that the mechanical integrity of the PEDOT layer was apparently maintained in all cases, since no fracture or crack was detected in the surface of the film. Note also that the remarkable influence of the charge (swelling) and discharge (shrinkage) processes experienced by the PEDOT layers on the structure of the external PLA layer is fully consistent with an actuation mechanism.

Once the mechanical and electrochemical properties of free-standing 5-pPLA/PEDOT membranes were proved, the electro-chemo-mechanical response was analyzed by applying square potential waves from ±0.6 to ±4.0 V during a period of time *t* (Figure S1), where *t*= 2, 4, 8 or 10 s. The positive voltage was held half of the time to oxidize the PEDOT layers (swelling), whereas the negative voltage was kept the same time to reduce them (shrinking). Although reversible bending displacements were successfully obtained for swelling-shrinking times examined, results discussed in this work have been focused on assays conducted using 10 s (*i.e.* 5 s for oxidation and 5s for reduction), since their monitoring was easier.

Figure 6a displays the experimental set up used to follow the movements of the free-standing 5-pPLA/PEDOT films. It is worth noting that the structural asymmetries caused by the templating effect exerted by PEDOT on pPLA layers, which essentially affect the roughness of the layer (*i.e.* 6±1, 90±14 and 103±9 nm for the 1st, 3rd and 5th pPLA layer, respectively) and the size of the nanoperforations (*i.e.* 49±14, 76±27 and 103±40 nm), facilitate the observed bending movements. The separate quantification of the angular displacement and the length variation, which are typically observed in self-standing and supported (*i.e.* thick bilayers) CP-containing actuators, respectively, is hindered by the co-existence of both kind of movements in 5-pPLA/PEDOT actuators. In addition, 5-pPLA/PEDOT films fold over themselves due to their sub-micrometric thickness and flexibility. In order to overcome these limitations, the global movement was quantified by photographing the film and comparing the variation in the film surface area (ΔA) from the recorded images.

Figure 6b displays the variation of ΔA with the potential. As it was expected, ΔA grows with the potential, increasing from 3.8%±0.9% for ±0.6 V to 28.0%±4.2% for ±4.0 V. The significant change described by the film is shown in Figure 6c, which present photographs on its voltammetric response to the studied potentials. The angle ($\Delta\alpha$) associated to bending movement at the different potentials is included in Figure 6c, while a short video showing the bending movement achieved using a voltage of ±2 V is provided in the ESI. The mechanical response of the 5-layered film upon consecutive swelling-shrinking processes was evaluated by applying consecutive square potential waves (up to 500) at the above mentioned potentials. Cyclability results, which are displayed in Figure 6d, indicate that the free-standing films remained intact when the square wave was ±0.6, ±1.0 and ±2.0 V. In contrast, films failed after 220±16 and

80±12 cycles when the potential was ±3.0 and ±4.0 V, respectively. Accordingly, next assays were conducted using a voltage ±2 V.

In order to evaluate the actuation force of the 5-pPLA/PEDOT film, the mass of the outer PLA layer was increased during the preparation process. More specifically, the spin-coating rate was decreased from 1200 rpm to 900, 600, 300 or 100 rpm. This represented an increment in the total mass of the films (Δm) comprised between 21%±8% (900 rpm) and 328%±35% (100 rpm) with respect to the film with the outer PLA layer prepared at 1200 rpm. Figure 6e, which represents the variation of ΔA against Δm when square voltage waves of ±2.0 V were applied for 10 s, shows that ΔA decreases with increasing Δm. However, such reduction is not pronounced when Δm < 120% and the bending movement is still appreciable when Δm is as high as 328%±35%. Overall, these results indicate that the 5-pPLA/PEDOT actuator is able to push a huge amount of mass (a video is provided in the ESI for the film with Δm= 135%).

In summary, CPs, especially PPy, have largely been studied as adequate materials for constructing actuators due to their property of oxidize and reduce in a reversible way. Such electrochemical reactions typically result into large angular displacements (up to 300º) when the actuator involves bilayer structures consisting of a thick tape or a plastic film with a thick CP layer on the right or the left side.[3,4,13] Alternatively, approaches based on thick self-supported CP films forming interpenetrated polymer networks[17-19,45] have been used as macroscopic tools able to translate the electrochemical reactions into film length variations. In both approaches, CP films are required to be thick enough to reach the working conditions without breaking. In contrast, the strategy presented in this work avoids mechanical failure by intercalating CP layers of ultra-thin thickness (*i.e.* the charge consumed during the electropolymerization was adjusted to 270 mC only, whereas thick CP films forming interpenetrated networks consumed > 25 C during the

electropolymerization[17-19,45]) between robust and elastic pPLA nanofilms. Moreover, self-supported 5-pPLA/PEDOT films exhibit bending movement without the assistance of any tape or thick plastic film adhered to it.

Although, direct comparison of angular displacement between thick bilayer structures and 5-pPLA/PEDOT membranes is precluded because of the thickness of the latter (*i.e.* ultra-thin 5-pPLA/PEDOT membranes tend to fold over themselves during the bending), the bending of this self-supported nanodevice instead of the classical length variations represents a significant improvement with respect to thick self-supported films forming interpenetrated polymer networks. Moreover, this bending is preserved after a very large number of cycles. On the other hand, triple layer PPy artificial muscles have been found to trail weights of up 180% the mass of CP,[46,47] while 5-pPLA/PEDOT films still exhibit appreciable bending when the mass of PLA, which is the most abundant component in the film, increases up to 328%±35%.

CONCLUSIONS

A novel actuator based on free-standing 5-layered films of submicrometric thickness (~0.7 μm) has been fabricated. The preparation process involves three spin-coated pPLA layers, which bring mechanical strength and flexibility, separated by two anodically polymerized PEDOT layers that provide the electrochemically response. These films were subjected to square potential waves to induce volumetric expansion and contraction of the PEDOT layers, causing reversible bending movements. The excellent performance of the developed Faradaic motor has been proved by observing movement when the total mass of the film increased up to 328% while the mass of conducting polymer is maintained. The utilization of two well-known biocompatible polymers, PLA and PEDOT, as unique components of the artificial muscle opens new

possibilities in the biomedical field in which both are currently employed for a huge number of biomedical applications.

ACKNOWLEDGEMENTS

Authors acknowledge MINECO-FEDER (RTI2018-098951-B-I00) and Agència de Gestió d'Ajuts Universitaris i de Recerca (2017SGR359) for financial support. Support for the research of C.A. was received through the prize "ICREA Academia" for excellence in research funded by the Generalitat de Catalunya. B. G. M. is thankful to CONACYT for the financial support through a postgraduate scholarship (328467 CVU 621314). J. J. Roa acknowledges the Serra Hunter program of the Generalitat de Catalunya. Authors are thanked to Prof. T. F. Otero (Universidad Politécnica de Cartagena, Spain) for his useful advises and recommendations.

REFERENCES

1. Otero, T. F.; Martinez, J. G.; Arias-Pardilla, J. Biomimetic Electrochemistry from Conducting Polymers. A Review: Artificial Muscles, Smart Membranes, Smart Drug Delivery and Computer/Neuron Interfaces. *Electrochim. Acta* **2012**, *84*, 112–128.
2. Otero, T. F. Coulovoltammetric and Dynamovoltammetric Responses from Conducting Polymers and Bilayer Muscles as Tools to Identify Reaction-driven Structural Changes. A Review. *Electrochim. Acta* **2016**, *212*, 440–457.
3. Pei, Q.; Inganas, O. Conjugated Polymers and the Bending Cantilever Method – Electrical Muscles and Smart Devices. *Adv. Mater. 1992, 4*, 277–278.

4. Otero, T.; Angulo, E.; Rodriguez, J.; Santamaria, C. Electrochemomechanical Properties from a Bilayer – Polypyrrole Nonconducting and Flexible Material Artificial Muscle. *J. Electroanal. Chem.* **1992**, *341*, 369–375.
5. Valero, L.; Arias-Pardilla, J.; Cauich-Rodríguez, J.; Smit, M. A.; Otero, T. F. Characterization of the Movement of Polypyrrole-Dodecylbenzenesulfonate-Perchlorate/Tape Artificial Muscles. Faradaic Control of Reactive Artificial Molecular Motors and Muscles. *Electrochim. Acta* **2011**, *56*, 3721-3726.
6. Beregoi, M.; Evanghelidis, A.; Diculescu, V. C.; Iovu, H.; Enculescu, I. Polypyrrole Actuator Based on Electrospun Microribbons. *ACS Appl. Mater. Interfaces* **2017**, *9*, 38068−38075.
7. Spinks, G. M.; Mottaghitalab, V.; Bahrami-Saniani, M.; Whitten, P. G.; Wallace, G. G. Carbon-Nanotube-Reinforced Polyaniline Fibers for High-Strength Artificial Muscles. *Adv. Mater.* **2006**, *18*, 637–640.
8. Mukai, K.; Asaka, K.; Hata, K.; Fernandez Otero, T.; Oike, H. High-Speed Carbon Nanotube Actuators Based on an Oxidation/Reduction Reaction. *Chem. Eur. J.* **2011**, *17*, 10965–10971.
9. Xie, X.; Qu, L.; Zhou, C.; Li, Y.; Zhu, J.; Bai, H.; Shi, G.; Dai, L. An Asymmetrically Surface-Modified Graphene Film Electrochemical Actuator. *ACSNano* **2010**, *4*, 6050–6054.
10. Liang, J.; Huang, Y.; Oh, J.; Kozlov, M.; Sui, D.; Fang, S.; Baughman, R. H.; Ma, Y.; Chen, Y. Electromechanical Actuators Based on Graphene and Graphene/Fe3O4 Hybrid Paper. *Adv. Funct. Mater.* **2011**, *21*, 3778–3784.
11. Jager, E. W. H.; Inganas, O.; Lundstrom, I. Microrobots for Micrometer-Size Objects in Aqueous Media: Potential Tools for Single-Cell Manipulation. *Science* **2000**, *288*, 2335–2338.

12. Jager, E. W. H.; Smela, E.; Inganas, O. Microfabricating Conjugated Polymer Actuators. *Science* **2000**, *290*, 1540–1545.
13. Higgins, S. J.; Lovell, K. V.; Rajapakse, R. M. G.; Walsby, N. M. Grafting and Electrochemical Characterisation of Poly-(3,4-ethylenedioxythiophene) Films, on Nafion and on Radiation-Grafted Polystyrenesulfonate–Polyvinylidene Fluoride Composite Surfaces. *J. Mater. Chem.* **2003**, *13*, 2485–2489.
14. Festin, N.; Plesse, C.; Pirim, P.; Chevrot, C.; Vidal, F. Electro-Active Interpenetrating Polymer Networks Actuators and Strain Sensors: Fabrication, Position Control and Sensing Properties. *Sens. Actuators B Chem.* **2014**, *193*, 82–88.
15. Vidal, F.; Popp, J. F.; Plesse, C.; Chevrot, C.; Teyssie, D. Feasibility of Conducting Semi-Interpenetrating Networks Based on a Poly(ethylene oxide) Network and Poly(3,4-ethylenedioxythiophene) in Actuator Design. *J. Appl. Polym. Sci.* **2003**, *90*, 3569–3577.
16. Plesse, C.; Vidal, F.; Teyssie, D.; Chevrot, C. Conducting Polymer Artificial Muscle Fibres: Toward an Open Air Linear Actuation. *Chem. Commun.* **2010**, *46*, 2910–2912.
17. Fuchiwaki, M.; Tanaka, K.; Kaneto, K. Planate Conducting Polymer Actuator Based on Polypyrrole and Its Application. *Sens. Actuators A Phys.* **2009**, *150*, 272–276.
18. Fuchiwaki, M.; Otero, T. F. Polypyrrole–*para*-phenolsulfonic Acid/Tape Artificial Muscle as a Tool to Clarify Biomimetic Driven Reactions and Ionic Exchanges. *J. Mater. Chem. B* **2014**, *2*, 1954–1965.

19. Fuchiwaki, M.; Martinez, J. G.; Otero, T. F. Polypyrrole Asymmetric Bilayer Artificial Muscle: Driven Reactions, Cooperative Actuation, and Osmotic Effects. *Adv. Funct. Mater.* **2015**, *25*, 1535–1541.
20. Stoyanov, H.; Kollosche, M.; McCarthy, D. N.; Kofod, G. Molecular Composites with Enhanced Energy Density for Electroactive Polymers. *J. Mater. Chem.* **2010**, *20*, 7558–7564.
21. Stoyanov, H.; Kollosche, M.; Risse, S.; Wache, R.; Kofod, G. Soft Conductive Elastomer Materials for Stretchable Electronics and Voltage Controlled Artificial Muscles. *Adv. Mater.* **2013**, *25*, 578–583.
22. Agrawal, A.; Chen, H.; Kim, H.; Zhu, B.; Adetiba, O.; Miranda, A.; Chipara, A. C.; Ajayan, P. M.; Jacot, J. G.; Verduzco, R. Electromechanically Responsive Liquid Crystal Elastomer Nanocomposites for Active Cell Culture. *ACS Macro Lett.* **2016**, *5*, 1386−1390.
23. Lee, Y.; Han, J.; Choi, B.; Yoon, J.; Park, H.; Kim, Y.; Lee, J.; Kim, D. H.; Kim, D. M.; Lim, M.; Kang, M.-H.; Kim, S.; Choi, S.-J. Three-Dimensionally Printed Micro-electromechanical Switches. *ACS Appl. Mater. Interfaces* **2018**, *10*, 15841−15846.
24. Otero, T. F.; Martinez, J. G. Physical and Chemical Awareness from Sensing Polymeric Artificial Muscles. Experiments and Modeling. *Prog. Polym. Sci.* **2015**, *44*, 62–78.
25. Yan, B.; Wu, Y.; Guo, L. Recent Advances on Polypyrrole Electroactuators. *Polymers* **2017**, *9*, 446.
26. Zhang, Q. M.; Serpe, M. J. Stimuli-Responsive Polymers for Actuation. *Chem. Phys. Chem.* **2017**, *18*, 1451–1465.

27. Mirvakili, S. M.; Hunter, I. W. Artificial Muscles: Mechanisms, Applications, and Challenges. *Adv. Mater.* **2018**, *30*, 1704407.

28. Tyler, B.; Gullotti, D.; Mangraviti, A.; Utsuki, T.; Brem, H. Polylactic Acid (PLA) Controlled Delivery Carriers for Biomedical Applications. *Adv. Drug Deliv. Rev.* **2016**, *107*, 163–175.

29. Li, X.; Wang, Y.; Guo, M.; Wang, Z. L.; Shao, N. N.; Zhang, P. B.; Chen, X. S.; Huang, Y. B. Degradable Three Dimensional-Printed Polylactic Acid Scaffold with Long-Term Antibacterial Activity. *ACS Sust. Chem. Eng.* **2018**, *6*, 2047–2054.

30. Xu, T.; Yang, H. Y.; Yang, D. Z.; Yu, Z. Z. Polylactic Acid Nanofiber Scaffold Decorated with Chitosan Islandlike Topography for Bone Tissue Engineering. *ACS Appl. Mater. Interfaces* **2017**, *9*, 21094–21104.

31. Hsu, S. H.; Chan, S. H.; Chiang, C. M.; Chen, C. C. C.; Jiang, C. F. Peripheral Nerve Regeneration Using a Microporous Polylactic Acid Asymmetric Conduit in a Rabbit Long-Gap Sciatic Nerve Transection Model. *Biomaterials* **2011**, *32*, 3764–3775.

32. Marzocchi, M.; Gualandi, I.; Calienni, M.; Zironi, I.; Scavetta, E.; Castellani, G.; Fraboni, B. Physical and Electrochemical Properties of PEDOT:PSS as a Tool for Controlling Cell Growth. *ACS Appl. Mater. Interfaces* **2015**, *7*, 17993–18003.

33. del Valle, L. J.; Estrany, F.; Armelin, E.; Oliver, R.; Alemán, C. Cellular Adhesion, Proliferation and Viability on Conducting Polymer Substrates. *Macromol. Biosci.* **2008**, *8*. 1144–1151.

34. Carli, S.; Fioravanti, G.; Armirotti, A.; Ciarpella, F.; Prato, M.; Ottonello, G.; Salerno, M.; Scarpellini, A.; Perrone, D.; Marchesi, E.; Ricci, D.; Fadiga, L. A New Drug Delivery System Based on Tauroursodeoxycholic Acid and PEDOT. *Chem. Eur. J.* **2019**, *9*, 2322–2329.

35. Puiggalí-Jou, A.; Micheletti, P.; Estrany, F.; del Valle, L. J.; Alemán, C. Electrostimulated Release of Neutral Drugs from Polythiophene Nanoparticles: Smart Regulation of Drug-Polymer Interactions. *Adv. Healthc. Mater.* **2017**, *6*, 1700453.

36. Li, P.; Zhang, S. P.; Li, K.; Wang, J. X.; Liu, M. L.; Gu, X. N.; Fan, Y. B. The Promoting Effect on Pre-osteoblast Growth Under Electrical and Magnetic Double Stimulation Based on PEDOT/Fe3O4/PLGA Magnetic-Conductive Bi-functional Scaffolds. *J. Mater. Chem. B* **2018**, *6*, 4952–4962.

37. Molina, B.; Cuesta, S.; Puiggalí-Jou, A.; del Valle, L. J.; Armelin, E.; Alemán, C. Perforated Polyester Nanomebranes as Templates of Electroactive and Robust Free-Standing Films. *Eur. Polym. J.* **2019**, *114*, 213–222.

38. Oliver, W. C.; Pharr, G. M. An Improved Technique for Determining Hardness and Elastic Modulus Using Load and Displacement Sensing Indentation Experiments. *J. Mater. Res.* **1992**, *7*, 1564–1583.

39. Oliver, W. C.; Pharr, G. M. Measurement of Hardness and Elastic Modulus by Instrumented Indentation: Advances in Understanding and Refinements to Methodology. *J. Mater. Res.* **2004**, *19*, 3–20.

40. Roa, J. J.; Fargas, G.; Mateo, A.; Jiménez-Piqué, E.; Dependence of Nanoindentation Hardness with Crystallographic Orientation of Austenite Grains in Metastable Stainless Steels. *Mat. Sci. Eng. A* **2015**, *645*, 188–195.

41. Tromas, C.; Stinville, J. C.; Templier, C.; Villechaise, P. ; Hardness and Elastic Modulus Gradients in Plasma-Nitrided 316L Polycrystalline Stainless Steel Investigated by Nanoindentation Tomography. *Acta Mater.* **2012**, *60*, 1965–1973.

42. Bec, S.; Tronck, A.; Loubet, J. L.; A Simple Guide to Determine Elastic Properties of Films on Substrate from Nanoindentation Experiments. *Phil. Mag.* **2006**, *86*, 5347–5358.

43. Pérez-Madrigal, M. M.; Edo, M. G.; Díaz, A.; Puiggalí, J.; Alemán, C. Poly-γ-glutamic Acid Hydrogels as Electrolyte for Poly(3,4-ethylenedioxythiophene)-Based. Supercapacitors. *J. Phys. Chem. C* **2017**, *121*, 3182–3193.

44. Pérez-Madrigal, M. M.; Estrany, F.; Armelin, E.; Díaz-Díaz, D.; Alemán C. Towards Sustainable Solid-State Supercapacitors: Electroactive Conducting Polymers Combined with Biohydrogels. *J. Mater. Chem. A* **2016**, *4*, 1792–1805.

45. Otero, T. F.; Martinez-Soria, L. X.; Schumacher, J.; Valero, L.; Pascual, V. H. Self-Supported Polypyrrole/Polyvinylsulfate Films: Electrochemical Synthesis, Characterization, and Sensing Properties of Their Redox Reactions. *ChemistryOpen* **2017**, *6*, 25–3.

46. Conzuelo, L. V.; Arias-Pardilla, J.; Cauich-Rodríguez, J. V.; Smit, M. A.; Otero, T. F. Sensing and Tactile Artificial Muscles from Reactive Materials. *Sensors* **2010**, *10*, 2638-2674.

47. Otero, T.F.; Cortes, M.T. Characterization of triple layers. *Smart Structures and Materials 2001: Electroactive Polymer Actuators and Devices,* Bellingham, WA, USA, 2001; pp. 93-100.

CAPTION TO FIGURES

Figure 1. (a) Reaction induced swelling/shrinking of a CP film. (b) Structure of the free-standing 5-layered 5-pPLA/PEDOT film.

Figure 2. Scheme illustrating the preparation of 5-pPLA/PEDOT free-standing membranes.

Figure 3. (a) Digital camera images displaying a scratched 5-pPLA/PEDOT membrane with an area of 3×2 cm^2 supported onto the steel substrate and three free standing 5-pPLA/PEDOT films (2×0.5 cm^2) floating in water. (b) Representative SEM micrograph of the surface of a supported 5-pPLA/PEDOT membrane. (c) SEM micrograph showing the transversal view of the self-standing membrane and representative EDX analyses of external PLA layer (blue circle) and the internal PEDOT-containing regions (red square).

Figure 4. Mechanical properties for both, a 5-pPLA/PEDOT membrane supported onto a steel substrate and the used steel, as a function of the displacement into surface: (a) hardness and (b) elastic modulus.

Figure 5. (a) Cyclic voltammograms recorded for a 5-pPLA/PEDOT film supported onto a steel substrate as it grows layer-by-layer. Scan rate: 100 mV/s. (b) First control voltammogram (black line) and voltammogram after 25 consecutive oxidation–reduction cycles (blue line) for a free-standing 5-pPLA/PEDOT film. The first control voltammogram recorded for a supported pPLA film is included for comparison (red line). (c) SEM micrograph of a 5-pPLA/PEDOT film after 25 consecutive oxidation–reduction cycles. (d) Curves for the first GCD cycles recorded at 0.75 mA for a free-standing 5-pPLA/PEDOT film. (e) Comparison of the 2^{nd} and 1500^{th} GCD cycles. (f) SEM micrograph of a free-standing 5-pPLA/PDOT film after 1500 consecutive GCD cycles.

Figure 6. (a) Experimental set up used to follow the movements of the free-standing 5-pPLA/PEDOT films. (b) Variation of the surface area (ΔA) against the voltage used for square potential waves. (c) Photographs displaying the response of free-standing 5-pPLA/PEDOT films against different voltages. The bending angle (Δα) at different potentials, which was measured from to the initial position at 0 V (white line) the position reached by the film at the desired potential (blue line), is also displayed. (d) Number of cycles that retain the mechanical integrity of the 5-pPLA/PEDOT film after apply up to 500 consecutive square potential waves using different voltages. (e) Variation of the surface area (ΔA) against the increment of mass for the outer pPLA layer (Δm) when square voltage waves of ±2.0 V were applied for 10 s.

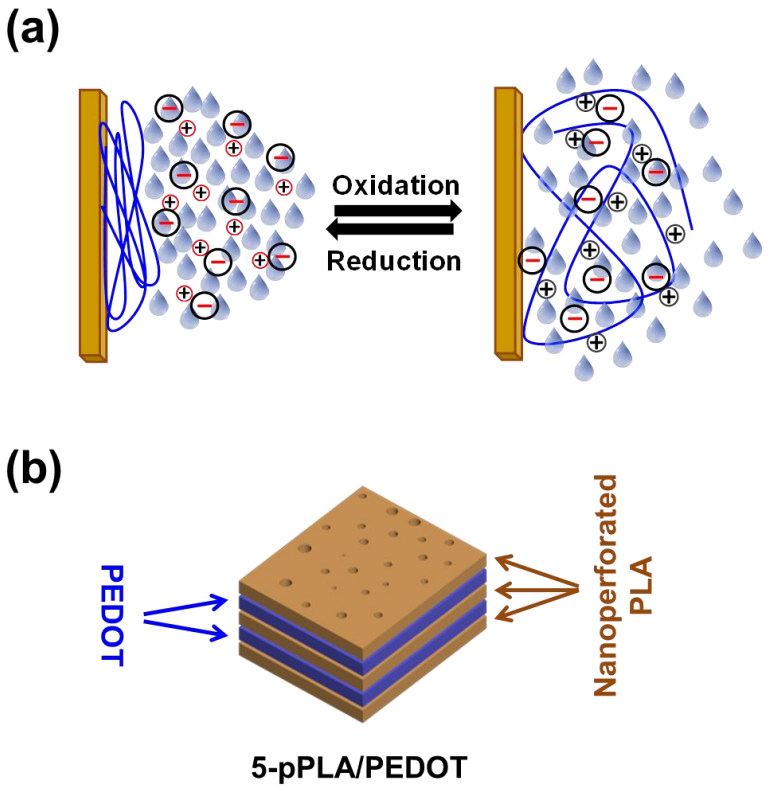
(a)
Oxidation
Reduction
(b)
PEDOT
Nanoperforated
PLA
5-pPLA/PEDOT

Figure 1

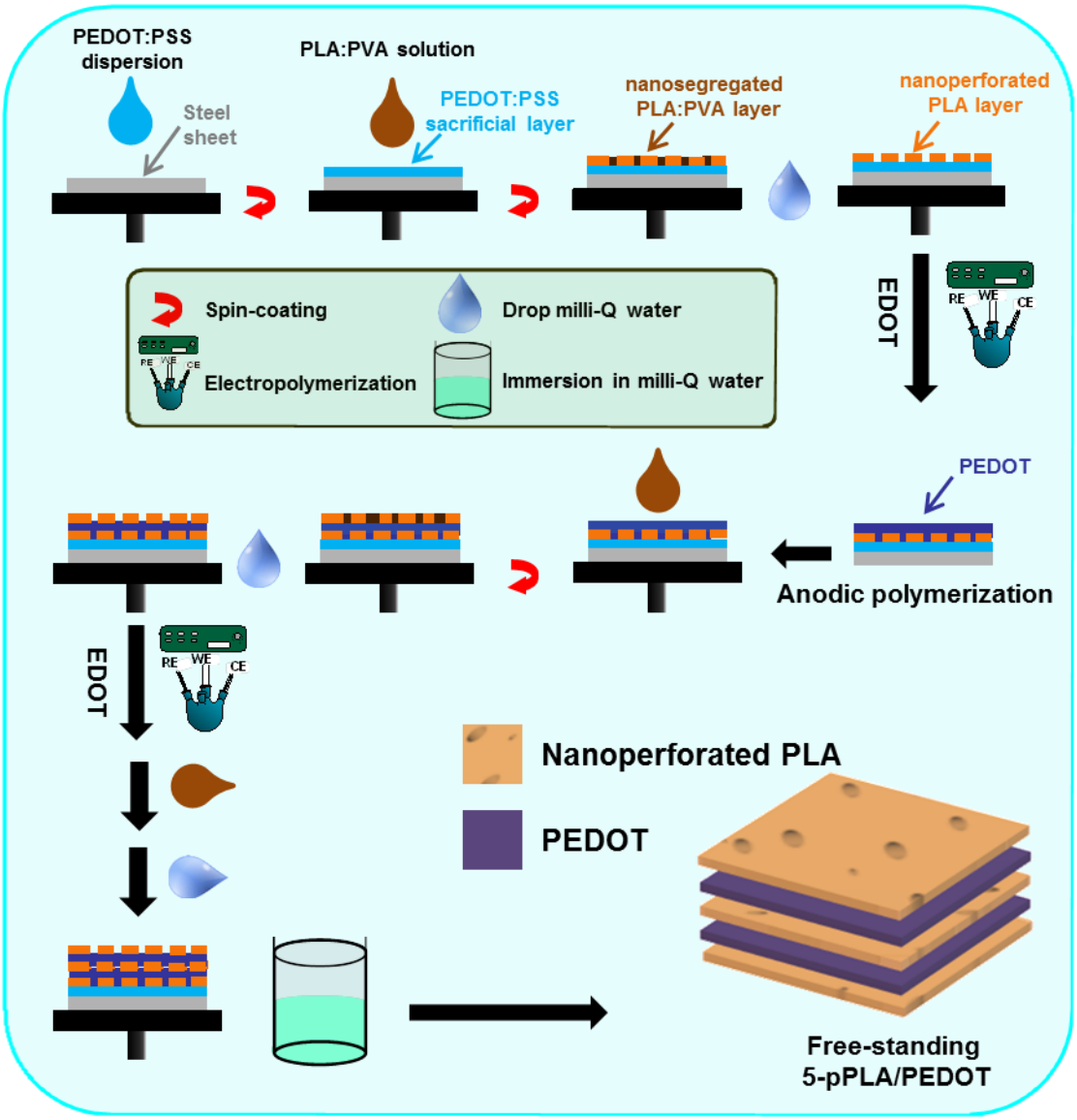
PEDOT:PSS dispersion
Steel sheet
PLA:PVA solution
PEDOT:PSS sacrificial layer
nanosegregated PLA:PVA layer
nanoperforated PLA layer
Spin-coating
Drop milli-Q water
Electropolymerization
Immersion in milli-Q water
EDOT
RE
WE
CE
PEDOT
Anodic polymerization
EDOT
Nanoperforated PLA
PEDOT
Free-standing 5-pPLA/PEDOT

Figure 2

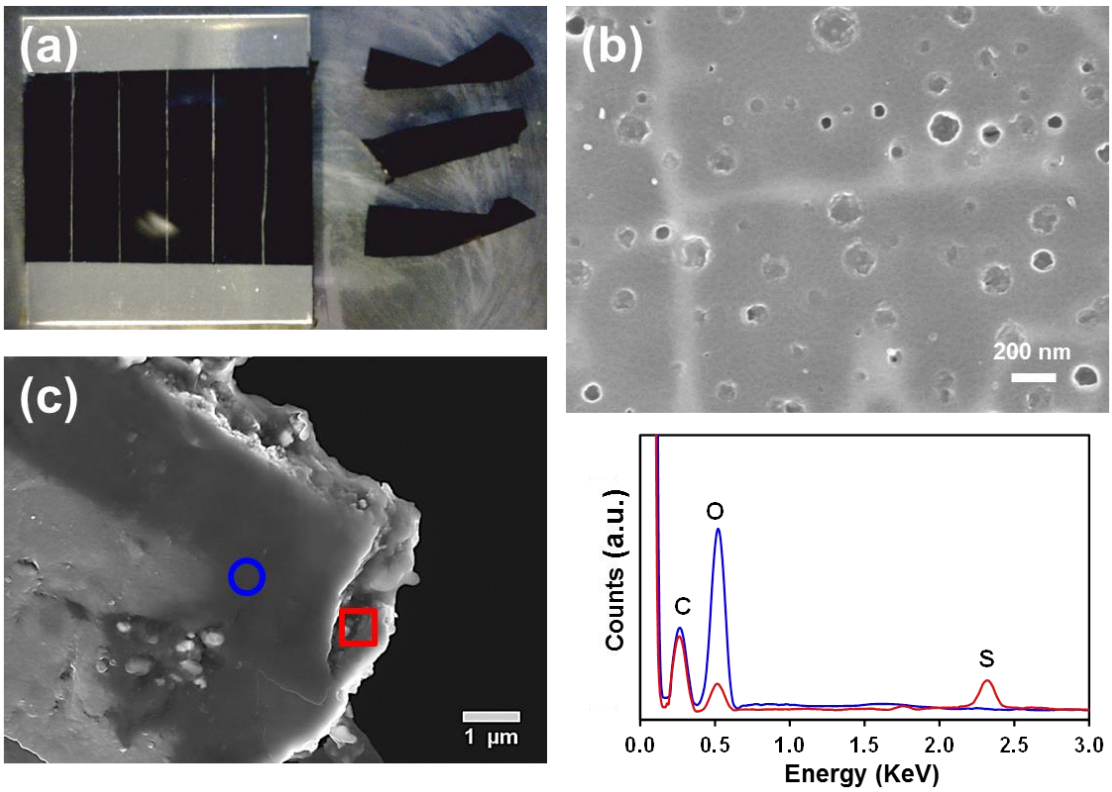

Figure 3

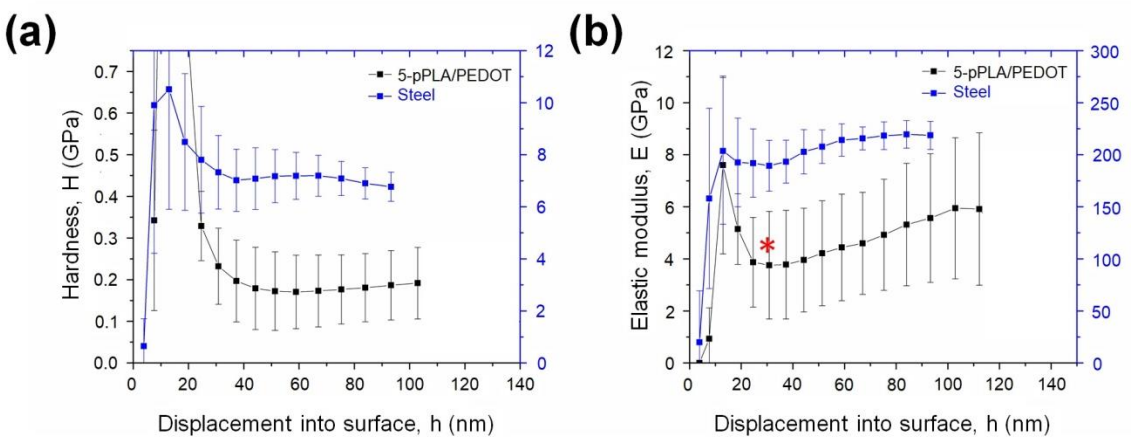
(a)
Hardness, H (GPa)
Displacement into surface, h (nm)
5-pPLA/PEDOT
Steel
(b)
Elastic modulus, E (GPa)
Displacement into surface, h (nm)
5-pPLA/PEDOT
Steel

Figure 4

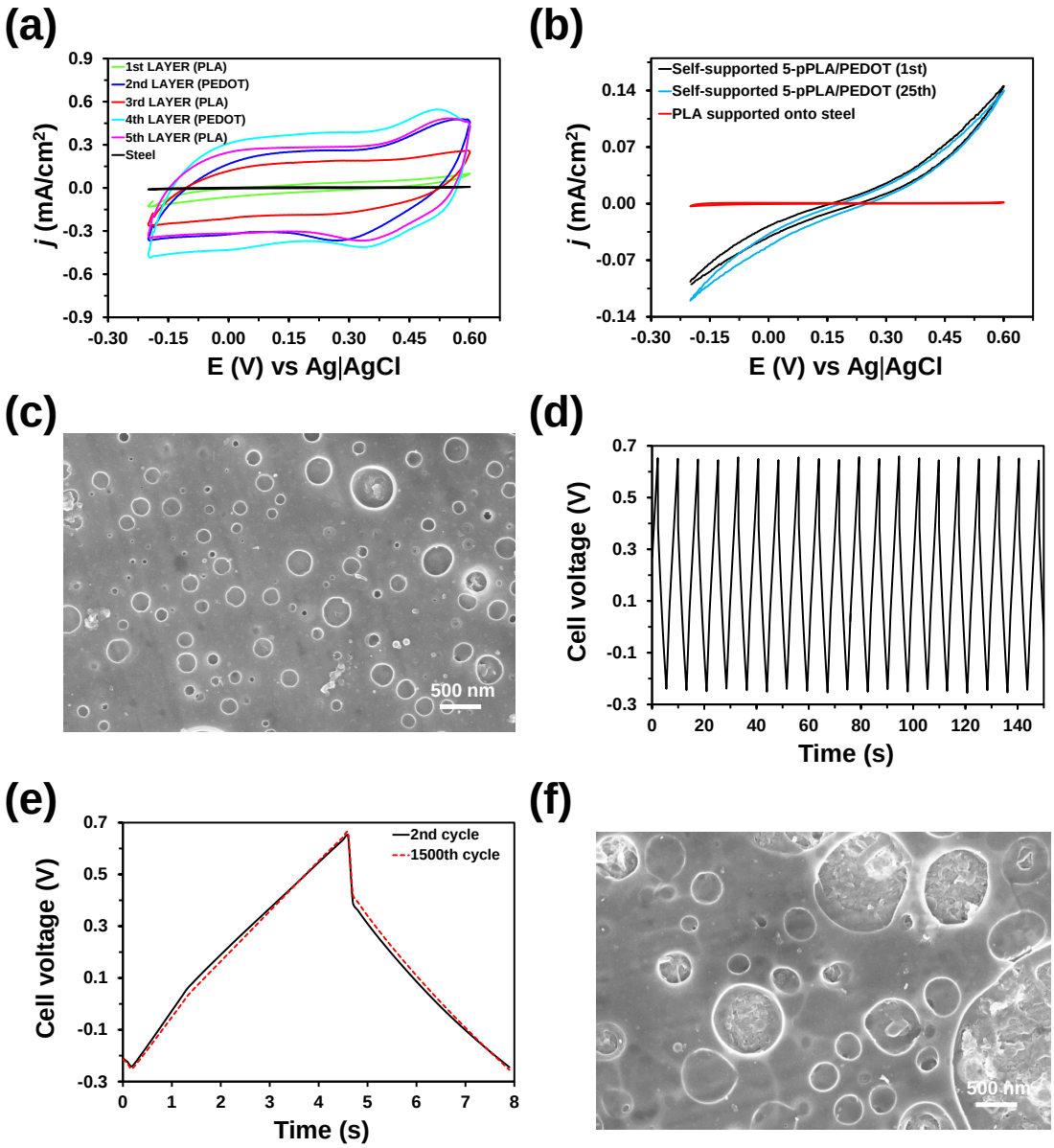
(a)
1st LAYER (PLA)
2nd LAYER (PEDOT)
3rd LAYER (PLA)
4th LAYER (PEDOT)
5th LAYER (PLA)
Steel
j (mA/cm²)
E (V) vs Ag|AgCl
(b)
Self-supported 5-pPLA/PEDOT (1st)
Self-supported 5-pPLA/PEDOT (25th)
PLA supported onto steel
j (mA/cm²)
E (V) vs Ag|AgCl
(c)
500 nm
(d)
Cell voltage (V)
Time (s)
(e)
2nd cycle
1500th cycle
Cell voltage (V)
Time (s)
(f)
500 nm

Figure 5

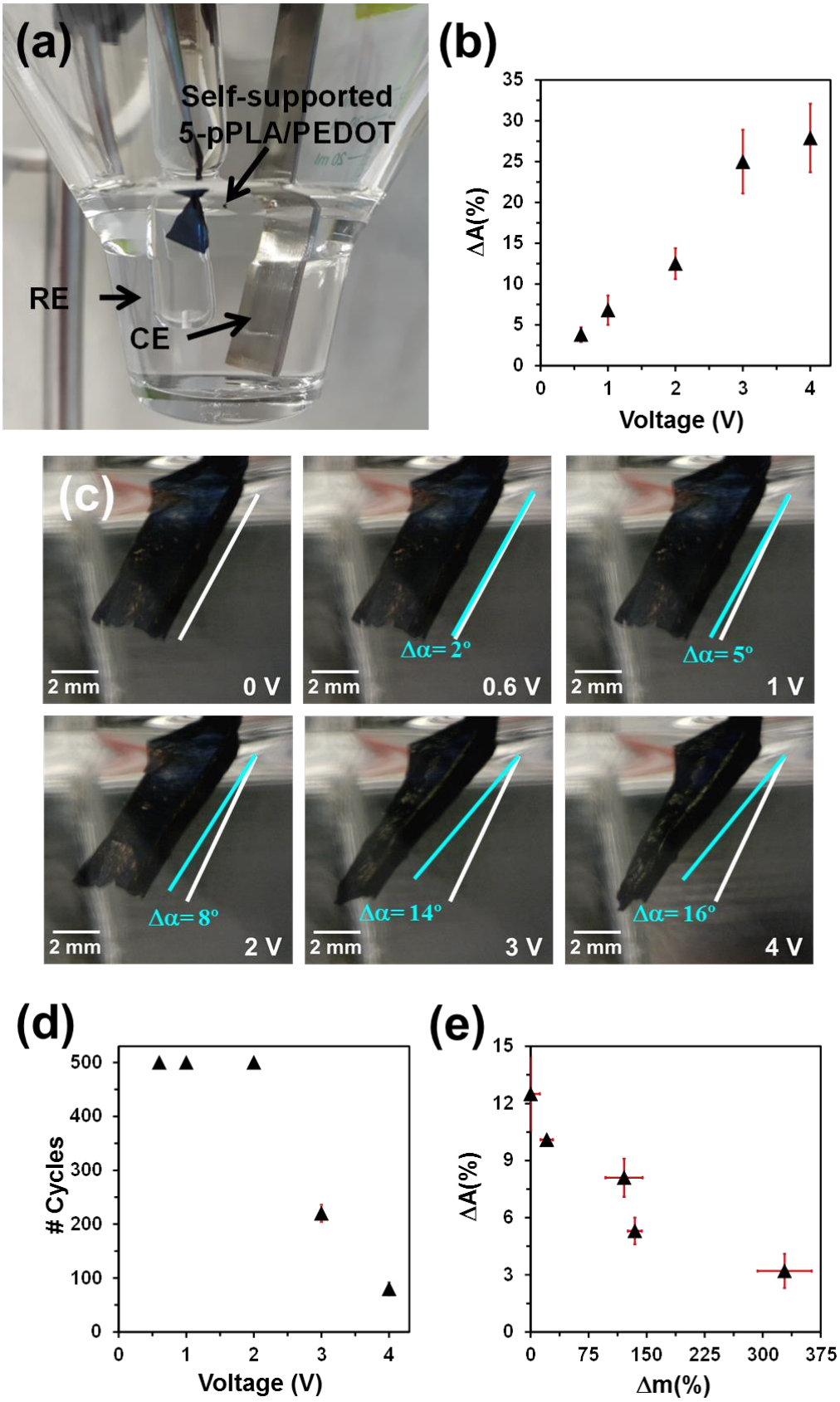
(a)
Self-supported
5-pPLA/PEDOT
RE
CE
(b)
ΔA(%)
Voltage (V)
(c)
2 mm
0 V
Δα= 2°
0.6 V
Δα= 5°
1 V
Δα= 8°
2 V
Δα= 14°
3 V
Δα= 16°
4 V
(d)
Cycles
Voltage (V)
(e)
ΔA(%)
Δm(%)

Figure 6

GRAPHICAL ABSTRACT